Cell Reports

Hippocampal Global Remapping Can Occur without Input from the Medial Entorhinal Cortex

Graphical Abstract

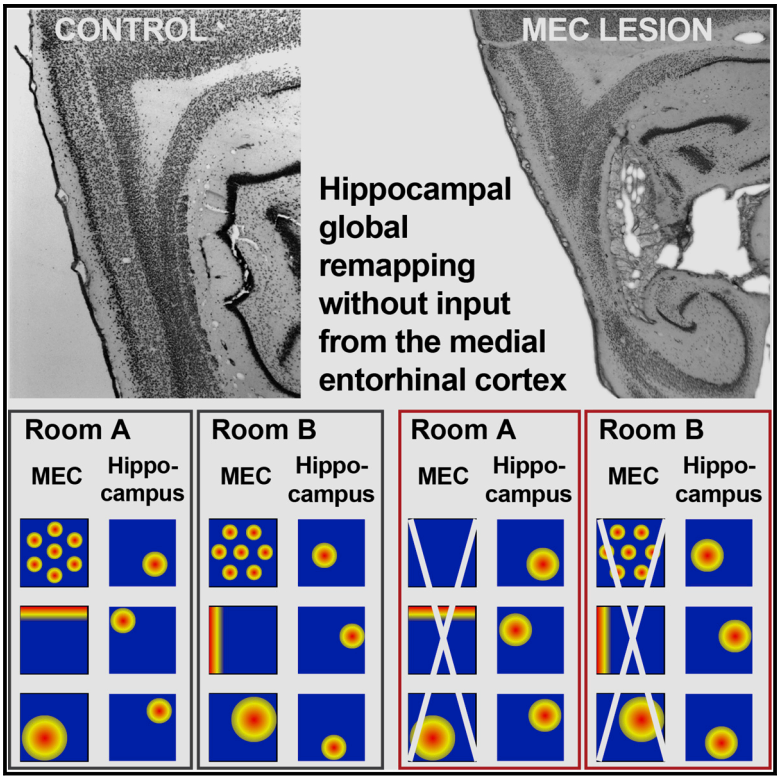

Highlights

- Hippocampal maps without mEC inputs are sufficiently stable to test for remapping
- Hippocampal global remapping is intact without mEC inputs
- Rapid generation of distinct hippocampal maps does not require mEC inputs
- Maps that form without mEC inputs in novel rooms stabilize within minutes

Authors

Magdalene I. Schlesiger, Brittney L. Boublil, Jena B. Hales, Jill K. Leutgeb, Stefan Leutgeb

Correspondence

sleutgeb@ucsd.edu

In Brief

Schlesiger et al. find that specialized spatial cells in mEC are not required for generating distinct hippocampal maps across environments. Inputs to the hippocampus, therefore, do not need to be specialized for spatial coding to support hippocampal spatial computations.

Schlesiger et al., 2018, Cell Reports *22*, 3152–3159
March 20, 2018
https://doi.org/10.1016/j.celrep.2018.02.082

CellPress

OPEN ACCESS
CellPress

Cell Reports
Report

Hippocampal Global Remapping Can Occur without Input from the Medial Entorhinal Cortex

Magdalene I. Schlesiger,[1,4] Brittney L. Boublil,[1] Jena B. Hales,[2] Jill K. Leutgeb,[1] and Stefan Leutgeb[1,3,5,*]
[1]Neurobiology Section and Center for Neural Circuits and Behavior, University of California, San Diego, La Jolla, CA 92093, USA
[2]Department of Psychological Sciences, University of San Diego, San Diego, CA 92110, USA
[3]Kavli Institute for Brain and Mind, University of California, San Diego, La Jolla, CA 92093, USA
[4]Present address: Department of Clinical Neurobiology, Medical Faculty of Heidelberg University and German Cancer Research Center (DKFZ), Heidelberg 69120, Germany
[5]Lead Contact
*Correspondence: sleutgeb@ucsd.edu
https://doi.org/10.1016/j.celrep.2018.02.082

SUMMARY

The high storage capacity of the episodic memory system relies on distinct representations for events that are separated in time and space. The spatial component of these computations includes the formation of independent maps by hippocampal place cells across environments, referred to as global remapping. Such remapping is thought to emerge by the switching of input patterns from specialized spatially selective cells in medial entorhinal cortex (mEC), such as grid and border cells. Although it has been shown that acute manipulations of mEC firing patterns are sufficient for inducing hippocampal remapping, it remains unknown whether specialized spatial mEC inputs are necessary for the reorganization of hippocampal spatial representations. Here, we examined remapping in rats without mEC input to the hippocampus and found that highly distinct spatial maps emerged rapidly in every individual rat. Our data suggest that hippocampal spatial computations do not depend on inputs from specialized cell types in mEC.

INTRODUCTION

The encoding of distinguishable episodic memories requires that neural representations for a multitude of places, contexts, and contents are generated with minimal overlap (Treves and Rolls, 1994). One fundamental component of this computation is the formation of distinct spatial maps by hippocampal place cells. Whereas place cells typically retain their firing locations within the same environment, minor changes to environmental features result in either rate changes without a spatial reorganization of place fields or in a partial reorganization of place field locations. In contrast, extended training across similar environments or exposure to highly distinct environments results in a reorganization of the spatial firing patterns of nearly all hippocampal cells (Muller and Kubie, 1987; Lever et al., 2002; Leutgeb et al., 2004, 2005; Alme et al., 2014). In the case when the resulting spatial representations across environments become maximally distinct, or orthogonal, this phenomenon is referred to as global remapping (Leutgeb et al., 2005).

It is widely assumed that the formation of distinct hippocampal maps depends on computations in the medial entorhinal cortex (mEC) (Buzsáki and Moser, 2013; Moser et al., 2014; Kanter et al., 2017), which sends projections to the hippocampus and contains functional cell types that are specialized in spatial coding, such as grid cells, border cells, directionally selective cells, and nongrid spatial cells (Köhler, 1985; Witter et al., 1988; Hafting et al., 2005; Sargolini et al., 2006; Solstad et al., 2008; Diehl et al., 2017; Hardcastle et al., 2017). The theory that mEC computations are part of the core mechanism for hippocampal global remapping is based on two lines of evidence. First, grid cells, border cells, and head direction cells rotate and shift their receptive fields between distinct environments and spatial nongrid cells alter their spatial firing patterns in response to differences in room configuration (Fyhn et al., 2007; Solstad et al., 2008; Diehl et al., 2017). These changes in mEC firing patterns occur along with hippocampal remapping, and it is therefore assumed that mEC provides the hippocampus with distinct spatial and directional information. Second, experimentally induced changes to mEC firing patterns have been shown to result in a spatial reorganization of hippocampal place fields (Miao et al., 2015; Rueckemann et al., 2016; Kanter et al., 2017). Taken together, these findings indicate that changes in mEC firing patterns are sufficient to cause hippocampal remapping.

The finding that mEC inputs are sufficient to induce remapping does not exclude the possibility that other inputs to hippocampus could also organize spatial maps. For example, numerous theoretical models point to the possibility that hippocampal map organization could be achieved independent of specialized mEC cells (O'Reilly and McClelland, 1994; Touretzky and Redish, 1996; Tsodyks et al., 1996; D'Albis et al., 2015; Grienberger et al., 2017). In support of the possibility that spatial firing is at least partially independent of mEC, studies that lesioned mEC or acutely inactivated mEC firing patterns found that hippocampal place fields persist (Hales et al., 2014; Schlesiger et al., 2013; Miao et al., 2015; Rueckemann et al., 2016; Kanter et al., 2017). The persistence of precise spatial firing while mEC inputs to hippocampus are diminished led to the notion that it is not the formation of spatial receptive fields but rather the selection of a particular map for each environment that is mEC dependent (Miao et al., 2015; Rueckemann et al., 2016). An implication of

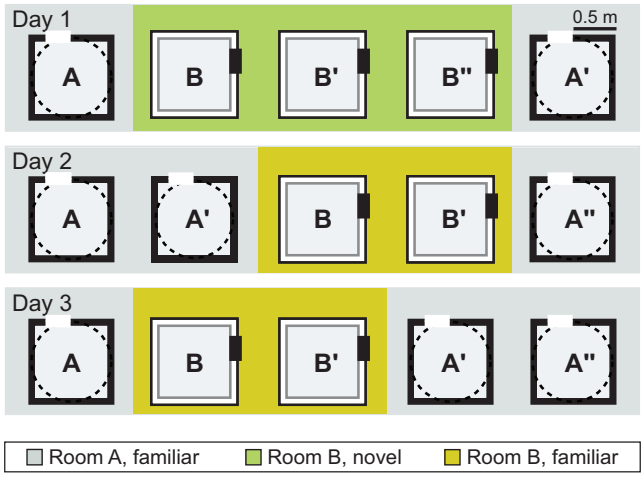

Figure 1. Experimental Design

Rats were trained to forage for randomly scattered chocolate sprinkles in open field arenas. Hippocampal recordings were performed over 3 days in two separate rooms on each day. One of the rooms was highly familiar at the beginning of the recording sequence (≥5 days of experience; referred to as room A), and one was novel on day 1 (referred to as room B). The recording environment in room A was either a squared enclosure with black walls or a circular enclosure with a black wall, and the recording environment in room B was a square enclosure with white walls. Each recording day consisted of five daily 10-min sessions with inter-session intervals of 5 min. On day 1, three consecutive sessions in room B were performed to examine map stability in the novel environment. On days 2 and 3, one of the recording sessions in room B was replaced with a room A recording to be able to compare map stability over two consecutive sessions in room A (e.g., A' and A'') and in room B (B' and B'').

this view would be that firing fields emerge independent of mEC but that their arrangement is fixed when map reorganization is no longer supported by mEC inputs. To address the question whether mEC is critical for hippocampal map selection, we first performed extensive, bilateral excitotoxic lesions of the mEC, which included up to 100% of mEC superficial layers, and then examined hippocampal remapping by recording from the CA1 region in freely behaving rats in two different environments. The advantage of permanent lesions compared to reversible manipulations (Südhof, 2015) is that the extent of the disrupted brain regions can be well quantified and does not change over the duration of the recording experiments, which excludes the possibility that the manipulation acutely alters mEC input patterns to the hippocampus and thereby directly contributes to remapping.

RESULTS

Complete Lesions of the mEC Superficial Layers

To determine whether mEC inputs are necessary for hippocampal global remapping, we performed either N-methyl-D-aspartate (NMDA) or sham lesions of mEC and recorded neuronal activity from CA1 cells in both hemispheres of the hippocampus. In order to exclude the possibility that any retained hippocampal function was the result of spared mEC tissue, we confirmed that our lesions included the entire dorsoventral extent of the mEC, including the grid cell area located in the dorsocaudal mEC (Hafting et al., 2005; Kerr et al., 2007). Stereological quantification of the lesion extent revealed up to 100% damage in the superficial layers of the mEC (percent damage: n = 5; layer II, median: 100.0%, range: 97.9%–100.0%; layer III, median: 92.4%, range: 68.6%–100.0%). If there was minor sparing, it occurred at the most ventro-lateral extent of mEC (Figure S1; see Hales et al., 2014 and Schlesiger et al., 2013 for additional photographs and detailed quantification of mEC lesions). Additional major damage was found in the dorsal and ventral parasubiculum (percent damage: medians: 78.0%–66%; ranges: 63.3%–85.8% and 31.0%–75.8%, respectively). Minor damage to lateral entorhinal cortex (lEC) along the border to mEC occurred in one of five rats, and minor damage to the ventral dentate gyrus was observed in one animal. Given that proximal and distal CA1 receive preferential input from mEC and lEC, respectively (Tamamaki and Nojyo, 1995; Witter et al., 2000; Naber et al., 2001), we additionally quantified the positions of our electrodes along the proximal-to-distal axis between CA2 and subiculum (Figures S1B and S1C). Whereas recording electrodes were distributed along the entire axis in control rats, they were preferentially confined to proximal CA1 in mEC-lesioned rats.

Hippocampal Place Fields Retained Spatial Selectivity without mEC Inputs

We examined hippocampal spatial firing by recording over 3 days in two separate rooms on each day (Figure 1). One of the two rooms was highly familiar (≥5 days of experience; referred to as room A), and the other was novel on day 1 of the recording sequence (referred to as room B). As previously reported (Schlesiger et al., 2013; Hales et al., 2014), we found that place fields remained clearly discernable in the mEC lesion group in both rooms (Figure 2A), even though place fields were larger and less informative compared to the control group (Figure S2A). We confirmed that the decrease in spatial precision was not a consequence of differences in recording quality between groups by examining standard cluster quality measures, which were similar between the mEC lesion and control group (Figure S3; L ratio, $p = 0.47$; isolation distance, $p = 0.84$; Mann-Whitney U tests). Despite the observed decrease in the spatial information scores of cells recorded in the mEC lesion group, firing rates of the active cell populations (mean firing rate ≥0.25 Hz) were similar between mEC lesion and control groups (Figure S2A). In addition, we found that the proportions of cells that were active in at least one of the rooms did not differ between the two groups (novel environment, control: 37/51 cells, mEC lesion: 51/80 cells; ≥5 days of experience, control: 48/78 cells, mEC lesion: 66/110 cells; both p values ≥ 0.37; chi-square tests). These results suggest that the change in spatial precision following the mEC lesion was not accompanied by a concurrent change in the average firing rates across the cell population.

Hippocampal Place Field Stability Was Partially Retained without Inputs from the mEC

We next examined whether place field locations were stable between sessions within the same room (Figures 2A and 2B) by computing the spatial correlations between pairs of rate maps from two consecutive recording sessions. As expected, control rats showed high map similarity in the highly familiar room

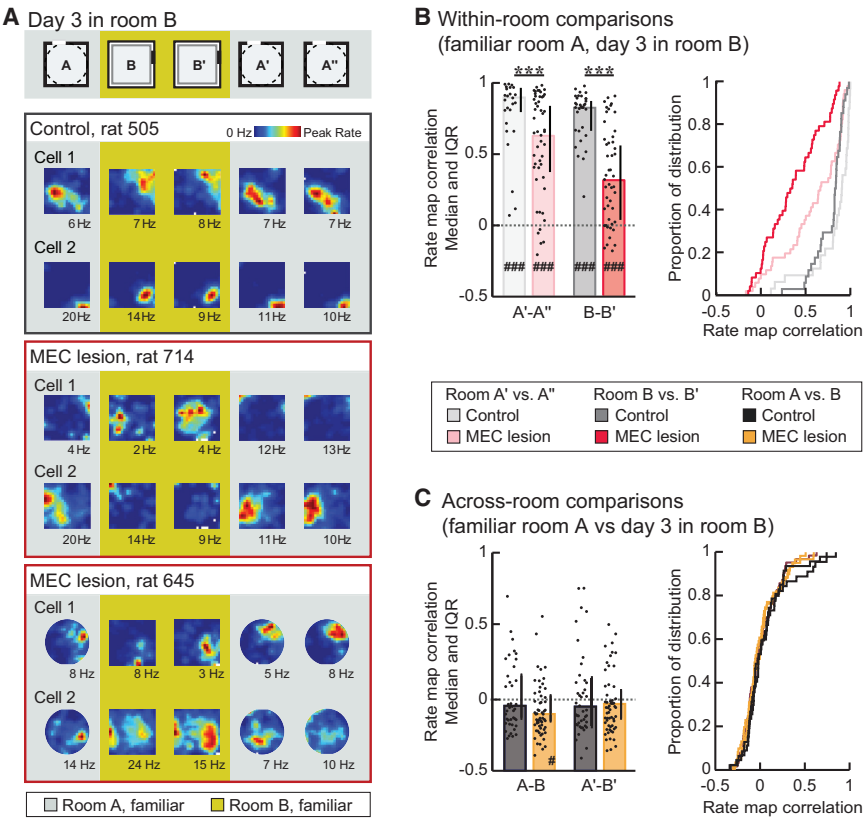

Figure 2. Map Stability between Repeated Sessions in the Same Room Was Reduced, but Remapping across Rooms Was Not Disrupted by mEC Lesions

(A) The rate map correlation between two consecutive sessions within and across rooms was analyzed in familiar rooms ($\geq$5 and $\geq$1 day of experience in room A and B, respectively). Hippocampal rate maps from representative simultaneously recorded example cells in control rat 505 and mEC-lesioned rats 714 and 645. The color scale is from 0 Hz (blue) to peak rate (red, indicated to the right of each session in Hz).

(B) Spatial correlations between pairs of consecutive sessions within the same room. Medians and inter-quartile range (IQR) (left panel) and cumulative distribution functions (right panel) are shown. Within-room map similarity was decreased in mEC-lesioned compared to control rats (p values < 0.001; MWU tests) but nonetheless remained above chance (i.e., the median of the shuffled distribution) for all comparisons (p values < 0.001; sign tests).

(C) Across-room map similarity was as low in the mEC lesion as in the control group (p values $\geq$ 0.24; MWU tests) and did not differ from chance for any comparison between rooms (all p values $\geq$ 0.35; sign tests) except for the first pair of sessions in the mEC lesion group (A-B), which showed a rate map correlation lower than chance (p = 0.0086). Error bars represent IQR, and black dots are values for individual cells. Dotted line indicates chance level. Holm-Bonferroni correction procedure was applied for multiple comparisons. mEC lesion versus control group, ***p $\leq$ 0.001; mEC lesion or control group versus shuffled distribution, #p $\leq$ 0.05 and ###p $\leq$ 0.001.
See Figure S1 for histology, Figure S2 for quantification of firing patterns within sessions, and Figure S3 for quantification of cluster stability.

(room A; $\geq$5 days of experience) as well as in the recently familiarized room (room B; 1 or 2 days of experience; median, 0.89 and 0.82, respectively; p = 0.65; χ^2 = 0.20; Friedman test). Rats in the mEC lesion group showed higher map stability in the highly familiar room than in the recently familiarized room (median, 0.65 and 0.33, respectively; p = 0.0065; χ^2 = 7.40; Friedman test) and lower map stability than controls in both conditions (both p values < 0.001; Mann-Whitney U tests). However, the remaining degree of stability was higher than what would be expected by chance for all comparisons, even when there was an intervening session in a different room (all p values < 0.001; sign tests with Holm-Bonferroni correction). There was therefore sufficient hippocampal map stability in our experimental conditions to test the contribution of the mEC to remapping across rooms.

To further examine the time course of map stabilization, we analyzed map stability within the first and within the second daily session in each environment (first versus second 5 min of a session; Figure S2B). Similar to the results obtained across sessions (Figure 2B), we found that within-session stability was lower in mEC-lesioned than in control rats in all sessions and environments (p values $\leq$ 0.0036; Mann-Whitney U tests). However, whereas the spatial firing patterns of control rats showed high stability within both the first and second session of a day, mEC-lesioned rats showed lower within-session stability during the first session compared to the second session irrespective of the familiarity of the environment (all p values $\leq$ 0.034; Wilcoxon signed-rank tests). Taken together, these results indicate that there was a short-term increase in stability in the MEC-lesioned group toward control levels within a recording day but that stabilized maps did not persist over longer time periods, such that each recording day in a familiar room started with stability levels that were as low as in a novel environment.

Global Remapping in Hippocampal CA1 Ensembles Did Not Require mEC Input

By next comparing pairs of rate maps between consecutive recording sessions in two different rooms, we observed that spatial maps reorganized to the same extent in the mEC lesion group as in the control group (Figure 2C; both p values $\geq$ 0.24; Mann-Whitney U tests). In both groups, the spatial correlation across rooms was similar to what would be expected by chance (all p values $\geq$ 0.35; sign tests) or was below chance (first pair of sessions in the mEC lesion group; p = 0.0086), confirming the formation of independent spatial maps for different spatial environments in both groups. In addition, map similarity for recordings across rooms was lower than for repeated recordings within the same room in both the mEC lesion and control group (both p values < 0.001; χ^2 $\geq$ 46.14; Friedman tests). Therefore, global remapping of CA1 ensembles between two familiar environments was intact after mEC lesions.

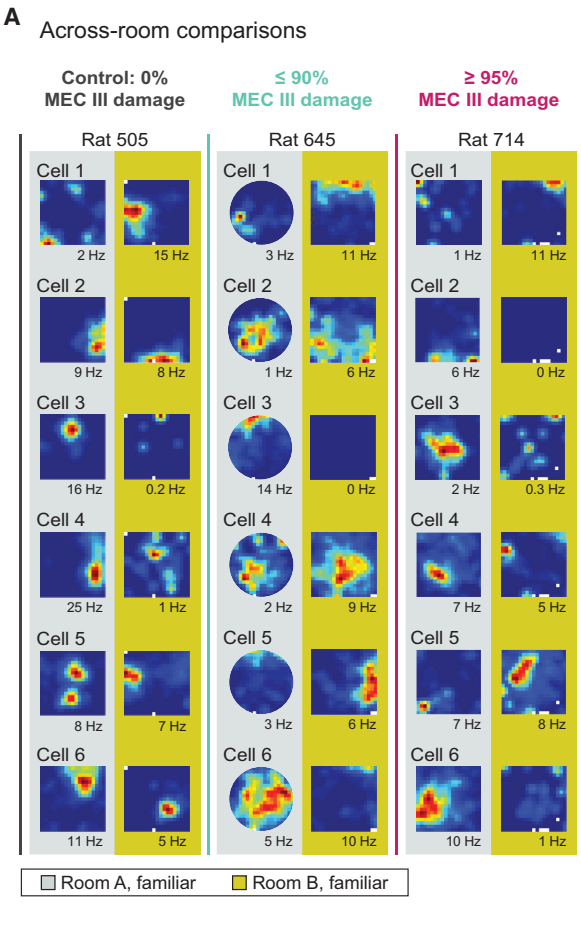

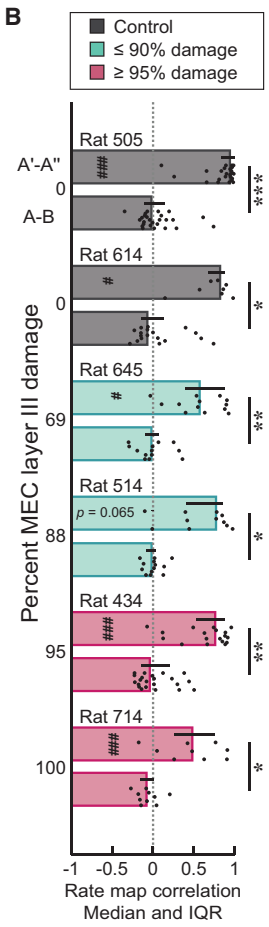

Figure 3. Global Remapping Was Intact in All mEC-Lesioned Rats, including Those with the Most Extensive Lesions

(A) Rate maps from representative example cells recorded in consecutive sessions across two different rooms are shown for rats with varying extent of damage to mEC layer III. Note that the amount of mEC layer II damage was ~100% in all mEC-lesioned rats. The color scale is from 0 Hz (blue) to peak rate (red, indicated to the right of each session in Hz).

(B) Remapping was intact in every individual rat. Within-room map similarity was higher than across-room map similarity for each rat in the control and mEC lesion group (all p values $\leq$ 0.047; MWU tests). Moreover, each rat showed across-room map similarity that was not different from chance (median of shuffled distribution; all p values $\geq$ 0.27; sign tests), whereas the within-room map similarity was higher than chance (all p values $\leq$ 0.016; sign tests) for all rats except for mEC-lesioned rat 714 (p = 0.065; sign test). Error bars represent IQR, and black dots are values for individual cells. Dotted line indicates chance level. Holm-Bonferroni correction procedure was applied for multiple comparisons. Within-room versus across-room comparison, *p $\leq$ 0.05, **p $\leq$ 0.005, and ***p $\leq$ 0.001; each rat versus shuffled distribution, #p $\leq$ 0.05 and ###p $\leq$ 0.001.

As not all of our lesions resulted in 100% elimination of the superficial layers, we also examined remapping of CA1 ensembles within individual rats (Figures 3A and 3B). The degree of remapping was similar across all rats, and individual rats in the mEC lesion and control groups remapped to the same extent (p = 0.82; χ^2 = 2.20; Kruskal-Wallis test). Moreover, in each individual control and mEC-lesioned rat, across-room map similarity did not differ from chance (all p values $\geq$ 0.27; sign tests) and was lower than the corresponding within-room comparison (all p values $\leq$ 0.047; Mann-Whitney U tests with Holm-Bonferroni correction). Of note, we confirmed that a rat with 100% bilateral damage to both mEC layer II and III retained global remapping comparable to controls (see rat 714 in Figures 2A, 3A, 3B, and S1), demonstrating that remapping in mEC-lesioned rats was not driven by spared mEC tissue.

In control rats, place field locations can be influenced by distal as well as proximal cues, such as the room geometry or a polarizing cue card (Fenton et al., 2000; Lee et al., 2004). In our experimental design, the orientation of the cue card was rotated across rooms (Figure 1) by either 90 or 270 degrees. This raises the possibility that the low map similarity observed in mEC-lesioned rats was not the result of a random redistribution of place field locations but instead emerged because the same spatial map was oriented to the new cue card. To test this possibility, we recalculated the correlations between pairs of rate maps obtained in different rooms after analytically rotating the map in the novel room according to the cue orientation (Figure S4A). We observed that the similarity between pairs of maps was not different from chance and did not differ between mEC-lesioned and control rats (Figure S4B). To account for the possibility that a constant map could be reoriented by any of the box walls or other shared properties between the two rooms, we also calculated the correlations between pairs of maps after rotating one of the maps in 90-degree steps (Figure S4A) and subsequently selecting the highest pairwise correlation for each cell. Using this method, we found that the scores for the mEC lesion and control group were not different from each other (both p values $\geq$ 0.65; Mann-Whitney U tests) and not different from chance (Figure S4B; all p values $\geq$ 0.37; sign tests). For both types of rotation analyses, corresponding results were also obtained when examining each rat individually (Figures S4C).

After confirming that maps did not simply rotate across rooms, we then more generally examined the possibility that map organization could have been retained across rooms. To this end, we calculated the distances between place field peaks of simultaneously recorded neurons (Figures 4A and 4B). We first established a baseline over repeated sessions in the same room and found that distances were retained across sessions in mEC-lesioned and control rats (p values < 0.001; r values $\geq$ 0.60; Pearson product-moment correlations), as would be expected if map geometry was corresponding. In contrast, distances

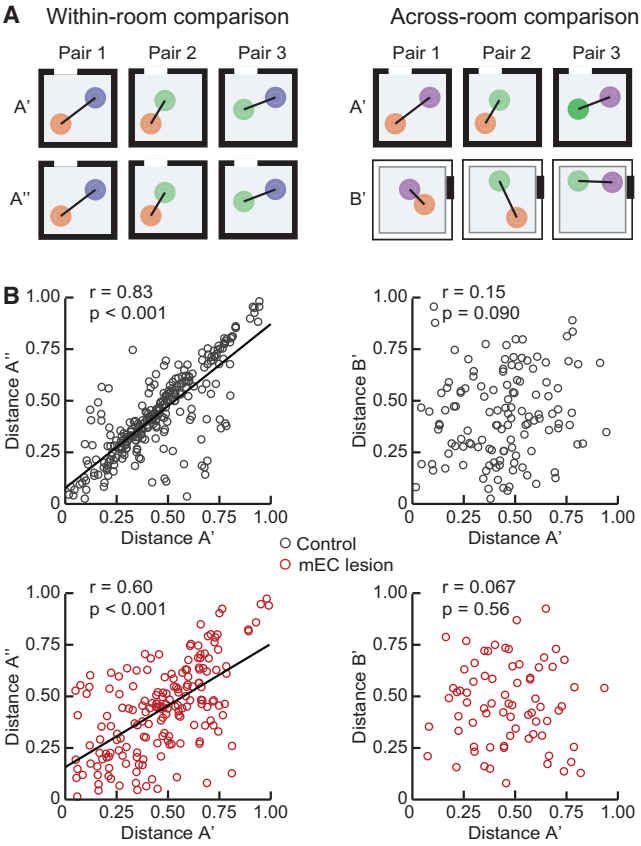

Figure 4. Place Field Distances Were Reorganized across Rooms in Both the mEC Lesion and the Control Group

The distances between place field peaks of pairs of simultaneously recorded cells were compared between two sessions within the same room (left) and across two different rooms (right).

(A) Schematic of expected distances between the place fields of three simultaneously recorded cells. Over consecutive recording sessions within the same room (A' and A''), place field distances are expected to be similar. In contrast, reorganization is expected to result in unrelated distances across two sessions in different rooms (A' and B').

(B) Over repeated sessions within the same room, place field peak distances were highly correlated in both control and mEC-lesioned rats (both p values < 0.001; both r values $\geq$ 0.60; Pearson product-moment correlations). Across rooms, distances were uncorrelated for both groups (p values $\geq$ 0.090; r values $\geq$ 0.15; Pearson product-moment correlations).

between place fields in one room were uncorrelated to the distances in the second room for both groups (p values $\geq$ 0.090; r values $\geq$ 0.15; Pearson product-moment correlations), which indicates that there were no preserved spatial relations.

Finally, we tested whether experience was required for distinct hippocampal representations to emerge after mEC lesions (Figure 5) by examining the place fields on day 1 of the recording series, when room B was novel to the rats (Figure 1). We first confirmed that stable maps were formed and retained in the novel room. We found that, for both control and mEC-lesioned rats, within-room map similarity was already above chance for the first pair of sessions in the novel room (Figures 5A and 5B; both p values $\leq$ 0.0020; sign tests). We then examined remapping between the familiar and novel rooms (Figure 5C) and found no difference between control and mEC-lesioned rats (both p values = 1.00; Mann-Whitney U tests). For both the control and mEC lesion group, the amount of correlation between maps for the different rooms did not exceed what would be expected by chance (all p values $\geq$ 0.13; sign tests). Moreover, the map similarity between consecutive sessions in different rooms was lower than the map similarity for consecutive recording sessions in the same room for both the mEC lesion and the control group (both p values $\leq$ 0.047; both X^2 values $\geq$ 1.57; Friedman tests). In the mEC lesion and control group, remapping thus occurred rapidly upon exposure to a novel environment.

DISCUSSION

It has been proposed that inputs from specialized cell types in the mEC are essential for the reorganization of hippocampal maps between different spatial environments (Monaco et al., 2011; Buzsáki and Moser, 2013; Kammerer and Leibold, 2014; Rowland and Moser, 2014; Miao et al., 2015). Whereas it has been shown that manipulations of mEC can result in hippocampal remapping, the previous studies did not ask whether mEC inputs are necessary for reorganizing hippocampal maps or whether the same function could also be performed without the highly specialized spatial and directional cell types that are found selectively in mEC. We addressed this question by recording hippocampal firing patterns in two different rooms in the absence of mEC input and found that highly distinct spatial maps emerged rapidly after exposure to a novel environment. The amount of rate map correlation between rooms was similar to what would be expected by chance and lower than during repeated recordings within the same room. Importantly, hippocampal global remapping was intact in each mEC-lesioned rat, even in individuals that had no detectable sparing of the superficial layers, which renders it unlikely that spared mEC input accounted for the formation of distinct hippocampal maps. Whereas mEC lesions did not preclude map formation in novel environments, the within-session stability of hippocampal place cells was decreased irrespective of room familiarity (Figure S2B). Therefore, our results indicate that map formation and map stabilization depend on separate entorhino-hippocampal circuits.

Since the discovery of remapping, it has been proposed that differences in the firing patterns of entorhinal cells are forwarded to the hippocampus, such that separate hippocampal maps emerge from the readout of this information (Muller and Kubie, 1987). Following the finding that hippocampal global remapping is accompanied by a coordinated shift in medial entorhinal grid cell firing patterns (Fyhn et al., 2007), this hypothesis was modified to suggest that the spatial reorganization of grid cells generates a redistribution of firing locations in the hippocampus (Monaco et al., 2011; Buzsáki and Moser, 2013; Kammerer and Leibold, 2014; Rowland and Moser, 2014; Miao et al., 2015). However, recent studies demonstrate that grid cells are not required for hippocampal global remapping (Brandon et al., 2014), raising the possibility that mEC cell types other than grid cells could provide distinct spatial information to the hippocampus. For example, it was recently shown that nongrid spatial cells

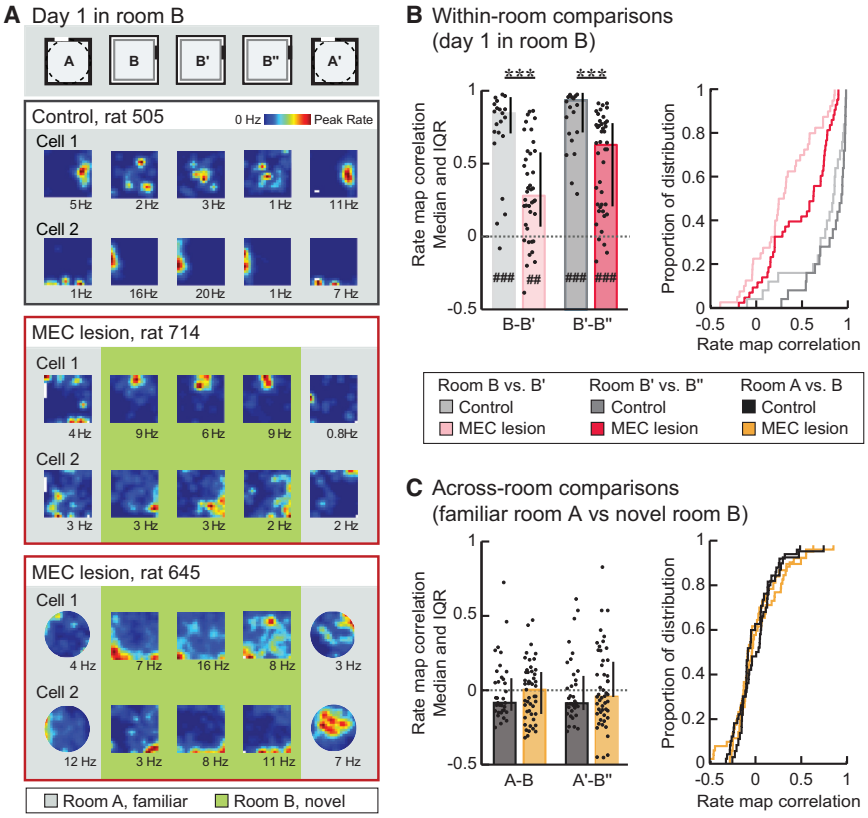

Figure 5. Distinct Hippocampal Maps Emerged Rapidly upon the First Exposure to a Novel Environment in Both mEC-Lesioned and Control Rats

Rate map correlations between consecutive sessions within and across rooms were analyzed on day 1 of the experiment, when room B was novel.

(A) Hippocampal rate maps from representative CA1 cells in control rat 505 and mEC-lesioned rats 714 and 645. The color scale is from 0 Hz (blue) to peak rate (red).

(B) Rate map correlations for pairs of consecutive sessions recorded within the same room. Medians and IQR (left panel) and cumulative distribution functions (right panel) are shown. Within-room map similarity in the mEC lesion group was lower than in the control group (p values < 0.001; MWU tests) but higher than chance (i.e., median of the shuffled distribution), even for the first pair of sessions in the novel room (all p values $\leq$ 0.0034; sign tests). The rate map correlation was higher for the second pair of sessions within the novel room (B'-B'') compared to the first pair of sessions in the novel room (B-B') for both the control and mEC lesion group (p values $\leq$ 0.030; Wilcoxon signed-rank tests).

(C) Across-room map similarity was as low in the mEC lesion as in the control group (both p values $\geq$ 1.00; MWU tests) and did not differ from chance in either group (all p values $\geq$ 0.13; sign tests).

Error bars represent IQR, and black dots are values for individual cells. Dotted line indicates chance level. Holm-Bonferroni correction procedure was applied for multiple comparisons. MEC lesion versus control group, ***$p \leq 0.001$; mEC lesion or control group versus shuffled distribution, ##$p \leq 0.005$ and ###$p \leq 0.001$. See Figure S4 for analysis of across-room map similarity that allows for box rotation.

remap in response to changes in environmental context (Diehl et al., 2017). Head direction cells and border cells are also known to distinguish environments with a coordinated rotation in their firing patterns and could thus be an additional contributor to hippocampal global remapping (Solstad et al., 2008). In addition to these correlative findings, acute manipulations of the mEC were shown to result in various degrees of hippocampal remapping (Miao et al., 2015; Rueckemann et al., 2016; Kanter et al., 2017). Taken together, these findings suggest that altered mEC inputs are sufficient to result in the formation of distinct spatial maps in the hippocampus.

Whereas previous studies that manipulated mEC firing patterns suggested that the mEC contributes to hippocampal remapping in the intact brain (Miao et al., 2015; Rueckemann et al., 2016; Kanter et al., 2017), they did not address whether the reorganization of hippocampal spatial maps requires highly specialized spatial and directional input from the mEC or whether spatial reorganization can also be achieved exclusively by the neuronal processing of less well-defined spatial inputs, for example, from the lEC (Hargreaves et al., 2005; Tsao et al., 2013). By performing extensive, bilateral mEC lesions that included up to 100% of the cells in the superficial layers, we tested whether mEC spatial inputs are necessary for the generation of new and distinct hippocampal maps. The lesion approach has the advantage that inputs from an entire brain region can be permanently eliminated before the experiment is performed. In contrast, optogenetic and chemogenetic inactivation techniques are known to not completely silence a target region and to allow for a compensatory increase of firing rates in a small population of cells. Such complex responses in the area that is targeted for inactivation would therefore not only reduce neuronal activity in mEC but also acutely alter the activity patterns during the recording experiment (Rueckemann et al., 2016; Miao et al., 2015; Kanter et al., 2017). Such acute manipulations can thus not answer the question whether mEC inputs are necessary for hippocampal remapping. However, our observation that global remapping is at control levels without sparing of the superficial layers allows for the conclusion that mEC is not required for hippocampal global remapping. These results are even more striking as recordings in mEC-lesioned rats were mostly obtained from proximal CA1, which would normally receive mEC input (Figures S1B and S1C). Anatomical adaptations, such as sprouting, or physiological adaptations, such as heightened responsiveness to CA3 inputs, may increase the contribution of the remaining entorhinal inputs to CA1, including inputs that reach CA1 indirectly through CA3 and dentate gyrus (DG). Although neuronal firing patterns in lEC are substantially less spatial than in mEC (Hargreaves et al., 2005), they nonetheless change across distinct contexts (Tsao et al., 2013; Keene et al., 2016). Our results thus raise the possibility that lEC

contributions are not limited to non-spatial modifications of the hippocampal maps, as has been concluded from a previous study with partial lEC lesions (Lu et al., 2013), but are also sufficient to reorganize spatial maps.

In addition to a possible contribution from lEC, it can also be speculated that hippocampal remapping could be induced more indirectly by the medial prefrontal cortex (mPFC). Cells in the mPFC strongly differentiate distinct spatial environments with firing rate changes and are additionally modulated by other task contingencies, such as the receipt of reward (Miyazaki et al., 2004; Hyman et al., 2005, 2012; Ito et al., 2015). Whereas a recent study demonstrated that medial prefrontal projections drive hippocampal rate remapping via the nucleus reunions of the thalamus (NR) (Ito et al., 2015), it is possible that the mPFC-NR pathway is also involved in the generation of global remapping. Future studies are needed to determine whether any of the inputs to hippocampus can generate distinct spatial maps as long as they provide sufficiently distinct patterns across environments. Irrespective of the nature of the alternative inputs to hippocampus that result in remapping in mEC-lesioned rats, our findings demonstrate that distinct hippocampal maps emerge without input from specialized cell types in the mEC and that weakly spatially selective inputs in combination with intrahippocampal processing are sufficient to result in a major spatial reorganization of the hippocampal map.

EXPERIMENTAL PROCEDURES

Further details and an outline of resources used in this work can be found in Supplemental Experimental Procedures.

Animals

Seven male adult Long-Evans rats were used for recordings from the hippocampal CA1 cell layer. Five received mEC lesions, and two received sham lesions. The mEC lesion extent was quantified in NeuN-stained sections. All experimental procedures were approved by the Institutional Animal Care and Use Committee at the University of California, San Diego.

Behavioral Procedures

Rats randomly foraged in up to 4 different environments with each environment placed in a different room. Over 3 consecutive days, a series of 10-min recording sessions was performed in two different rooms on each day (Figure 1). One of the two rooms was familiar to the rats, whereas the second room was novel to the rats at the beginning of the recording sequence.

Data Analysis

All data analysis was performed by importing position and spike data into MATLAB and by further processing the data with custom-written scripts and functions. Spike sorting was performed manually using the graphical cluster-cutting software (MClust, D. Redish), which we modified in order to reliably track clusters across sessions. Spatial firing rate distributions were constructed for 5 cm by 5 cm bins and by smoothing with a Gaussian filter with a SD of approximately 1 bin. The spatial information was calculated for the rate map of each session, and spatial similarity between rate maps was compared across sessions using Pearson's correlation. In addition, the distances between place field peaks were calculated for each pair of simultaneously recorded cells when each cell in the pair had at least one field.

Statistical Analysis

All statistical tests were two sided with $\alpha = 0.05$. Proportions were compared with chi-square tests. For all remaining statistical analysis, Kolmogorov-Smirnov tests were first performed to test for normality. Because all distributions were non-normal, Mann-Whitney U (MWU) tests and Kruskal-Wallis tests were used for between-group comparisons and Wilcoxon signed-rank tests and Friedman tests for within-group comparisons. Sign tests were used to test the samples against chance. Multiple comparisons were corrected with the Holm-Bonferroni procedure, and Tukey-Kramer tests were used for post hoc analysis.

DATA AND SOFTWARE AVAILABILITY

MClust software is freely available from A.D. Redish at http://redishlab.neuroscience.umn.edu/MClust/MClust.html. Reasonable requests for data and for software will be fulfilled by the lead contact.

SUPPLEMENTAL INFORMATION

Supplemental Information includes Supplemental Experimental Procedures and four figures and can be found with this article online at https://doi.org/10.1016/j.celrep.2018.02.082.

ACKNOWLEDGMENTS

The authors thank Mandy Wong for technical assistance. This work was supported by a Boehringer Ingelheim Fonds PhD fellowship, Walter F. Heiligenberg Professorship, and NIH grants R01 NS086947, R01 NS084324, and R01 MH100349.

AUTHOR CONTRIBUTIONS

Conceptualization, M.I.S., S.L., and J.K.L.; Methodology, M.I.S., S.L., and J.K.L.; Investigation, M.I.S., B.L.B., and J.B.H.; Formal Analysis, M.I.S.; Writing, M.I.S., S.L., and J.K.L.; Funding Acquisition, M.I.S., S.L., and J.K.L.

DECLARATION OF INTERESTS

The authors declare no competing interests.

Received: June 27, 2017
Revised: December 26, 2017
Accepted: February 21, 2018
Published: March 20, 2018

REFERENCES

Alme, C.B., Miao, C., Jezek, K., Treves, A., Moser, E.I., and Moser, M.B. (2014). Place cells in the hippocampus: eleven maps for eleven rooms. Proc. Natl. Acad. Sci. USA *111*, 18428–18435.

Brandon, M.P., Koenig, J., Leutgeb, J.K., and Leutgeb, S. (2014). New and distinct hippocampal place codes are generated in a new environment during septal inactivation. Neuron *82*, 789–796.

Buzsáki, G., and Moser, E.I. (2013). Memory, navigation and theta rhythm in the hippocampal-entorhinal system. Nat. Neurosci. *16*, 130–138.

D'Albis, T., Jaramillo, J., Sprekeler, H., and Kempter, R. (2015). Inheritance of hippocampal place fields through hebbian learning: effects of theta modulation and phase precession on structure formation. Neural Comput. *27*, 1624–1672.

Diehl, G.W., Hon, O.J., Leutgeb, S., and Leutgeb, J.K. (2017). Grid and nongrid cells in medial entorhinal cortex represent spatial location and environmental features with complementary coding schemes. Neuron *94*, 83–92.e6.

Fenton, A.A., Csizmadia, G., and Muller, R.U. (2000). Conjoint control of hippocampal place cell firing by two visual stimuli. Ii. A vector-field theory that predicts modifications of the representation of the environment. J. Gen. Physiol. *116*, 211–221.

Fyhn, M., Hafting, T., Treves, A., Moser, M.B., and Moser, E.I. (2007). Hippocampal remapping and grid realignment in entorhinal cortex. Nature *446*, 190–194.

Grienberger, C., Milstein, A.D., Bittner, K.C., Romani, S., and Magee, J.C. (2017). Inhibitory suppression of heterogeneously tuned excitation enhances spatial coding in CA1 place cells. Nat. Neurosci. *20*, 417–426.

Hafting, T., Fyhn, M., Molden, S., Moser, M.B., and Moser, E.I. (2005). Microstructure of a spatial map in the entorhinal cortex. Nature *436*, 801–806.

Hales, J.B., Schlesiger, M.I., Leutgeb, J.K., Squire, L.R., Leutgeb, S., and Clark, R.E. (2014). Medial entorhinal cortex lesions only partially disrupt hippocampal place cells and hippocampus-dependent place memory. Cell Rep. *9*, 893–901.

Hardcastle, K., Ganguli, S., and Giocomo, L.M. (2017). Cell types for our sense of location: where we are and where we are going. Nat. Neurosci. *20*, 1474–1482.

Hargreaves, E.L., Rao, G., Lee, I., and Knierim, J.J. (2005). Major dissociation between medial and lateral entorhinal input to dorsal hippocampus. Science *308*, 1792–1794.

Hyman, J.M., Zilli, E.A., Paley, A.M., and Hasselmo, M.E. (2005). Medial prefrontal cortex cells show dynamic modulation with the hippocampal theta rhythm dependent on behavior. Hippocampus *15*, 739–749.

Hyman, J.M., Ma, L., Balaguer-Ballester, E., Durstewitz, D., and Seamans, J.K. (2012). Contextual encoding by ensembles of medial prefrontal cortex neurons. Proc. Natl. Acad. Sci. USA *109*, 5086–5091.

Ito, H.T., Zhang, S.J., Witter, M.P., Moser, E.I., and Moser, M.B. (2015). A prefrontal-thalamo-hippocampal circuit for goal-directed spatial navigation. Nature *522*, 50–55.

Kammerer, A., and Leibold, C. (2014). Hippocampal remapping is constrained by sparseness rather than capacity. PLoS Comput. Biol. *10*, e1003986.

Kanter, B.R., Lykken, C.M., Avesar, D., Weible, A., Dickinson, J., Dunn, B., Borgesius, N.Z., Roudi, Y., and Kentros, C.G. (2017). A novel mechanism for the grid-to-place cell transformation revealed by transgenic depolarization of medial entorhinal cortex layer II. Neuron *93*, 1480–1492.e6.

Keene, C.S., Bladon, J., McKenzie, S., Liu, C.D., O'Keefe, J., and Eichenbaum, H. (2016). Complementary functional organization of neuronal activity patterns in the perirhinal, lateral entorhinal, and medial entorhinal cortices. J. Neurosci. *36*, 3660–3675.

Kerr, K.M., Agster, K.L., Furtak, S.C., and Burwell, R.D. (2007). Functional neuroanatomy of the parahippocampal region: the lateral and medial entorhinal areas. Hippocampus *17*, 697–708.

Köhler, C. (1985). Intrinsic projections of the retrohippocampal region in the rat brain. I. The subicular complex. J. Comp. Neurol. *236*, 504–522.

Lee, I., Yoganarasimha, D., Rao, G., and Knierim, J.J. (2004). Comparison of population coherence of place cells in hippocampal subfields CA1 and CA3. Nature *430*, 456–459.

Leutgeb, S., Leutgeb, J.K., Treves, A., Moser, M.B., and Moser, E.I. (2004). Distinct ensemble codes in hippocampal areas CA3 and CA1. Science *305*, 1295–1298.

Leutgeb, S., Leutgeb, J.K., Barnes, C.A., Moser, E.I., McNaughton, B.L., and Moser, M.B. (2005). Independent codes for spatial and episodic memory in hippocampal neuronal ensembles. Science *309*, 619–623.

Lever, C., Wills, T., Cacucci, F., Burgess, N., and O'Keefe, J. (2002). Long-term plasticity in hippocampal place-cell representation of environmental geometry. Nature *416*, 90–94.

Lu, L., Leutgeb, J.K., Tsao, A., Henriksen, E.J., Leutgeb, S., Barnes, C.A., Witter, M.P., Moser, M.B., and Moser, E.I. (2013). Impaired hippocampal rate coding after lesions of the lateral entorhinal cortex. Nat. Neurosci. *16*, 1085–1093.

Miao, C., Cao, Q., Ito, H.T., Yamahachi, H., Witter, M.P., Moser, M.B., and Moser, E.I. (2015). Hippocampal remapping after partial inactivation of the medial entorhinal cortex. Neuron *88*, 590–603.

Miyazaki, K., Miyazaki, K.W., and Matsumoto, G. (2004). Different representation of forthcoming reward in nucleus accumbens and medial prefrontal cortex. Neuroreport *15*, 721–726.

Monaco, J.D., Knierim, J.J., and Zhang, K. (2011). Sensory feedback, error correction, and remapping in a multiple oscillator model of place-cell activity. Front. Comput. Neurosci. *5*, 39.

Moser, E.I., Roudi, Y., Witter, M.P., Kentros, C., Bonhoeffer, T., and Moser, M.B. (2014). Grid cells and cortical representation. Nat. Rev. Neurosci. *15*, 466–481.

Muller, R.U., and Kubie, J.L. (1987). The effects of changes in the environment on the spatial firing of hippocampal complex-spike cells. J. Neurosci. *7*, 1951–1968.

Naber, P.A., Lopes da Silva, F.H., and Witter, M.P. (2001). Reciprocal connections between the entorhinal cortex and hippocampal fields CA1 and the subiculum are in register with the projections from CA1 to the subiculum. Hippocampus *11*, 99–104.

O'Reilly, R.C., and McClelland, J.L. (1994). Hippocampal conjunctive encoding, storage, and recall: avoiding a trade-off. Hippocampus *4*, 661–682.

Rowland, D.C., and Moser, M.B. (2014). From cortical modules to memories. Curr. Opin. Neurobiol. *24*, 22–27.

Rueckemann, J.W., DiMauro, A.J., Rangel, L.M., Han, X., Boyden, E.S., and Eichenbaum, H. (2016). Transient optogenetic inactivation of the medial entorhinal cortex biases the active population of hippocampal neurons. Hippocampus *26*, 246–260.

Sargolini, F., Fyhn, M., Hafting, T., McNaughton, B.L., Witter, M.P., Moser, M.B., and Moser, E.I. (2006). Conjunctive representation of position, direction, and velocity in entorhinal cortex. Science *312*, 758–762.

Schlesiger, M.I., Cressey, J.C., Boublil, B., Koenig, J., Melvin, N.R., Leutgeb, J.K., and Leutgeb, S. (2013). Hippocampal activation during the recall of remote spatial memories in radial maze tasks. Neurobiol. Learn. Mem. *106*, 324–333.

Solstad, T., Boccara, C.N., Kropff, E., Moser, M.B., and Moser, E.I. (2008). Representation of geometric borders in the entorhinal cortex. Science *322*, 1865–1868.

Südhof, T.C. (2015). Reproducibility: experimental mismatch in neural circuits. Nature *528*, 338–339.

Tamamaki, N., and Nojyo, Y. (1995). Preservation of topography in the connections between the subiculum, field CA1, and the entorhinal cortex in rats. J. Comp. Neurol. *353*, 379–390.

Touretzky, D.S., and Redish, A.D. (1996). Theory of rodent navigation based on interacting representations of space. Hippocampus *6*, 247–270.

Treves, A., and Rolls, E.T. (1994). Computational analysis of the role of the hippocampus in memory. Hippocampus *4*, 374–391.

Tsao, A., Moser, M.B., and Moser, E.I. (2013). Traces of experience in the lateral entorhinal cortex. Curr. Biol. *23*, 399–405.

Tsodyks, M.V., Skaggs, W.E., Sejnowski, T.J., and McNaughton, B.L. (1996). Population dynamics and theta rhythm phase precession of hippocampal place cell firing: a spiking neuron model. Hippocampus *6*, 271–280.

Witter, M.P., Holtrop, R., and Van de Loosdrecht, A.A. (1988). Direct projections from the periallocortical subicular complex to the fascia dentata in the rat. An anatomical tracing study using *Phaseolus vulgaris* leucoagglutinin. Neurosci. Res. Commun. *2*, 61–68.

Witter, M.P., Naber, P.A., van Haeften, T., Machielsen, W.C., Rombouts, S.A., Barkhof, F., Scheltens, P., and Lopes da Silva, F.H. (2000). Cortico-hippocampal communication by way of parallel parahippocampal-subicular pathways. Hippocampus *10*, 398–410.

Cell Reports, Volume *22*

Supplemental Information

Hippocampal Global Remapping Can Occur without Input from the Medial Entorhinal Cortex

Magdalene I. Schlesiger, Brittney L. Boublil, Jena B. Hales, Jill K. Leutgeb, and Stefan Leutgeb

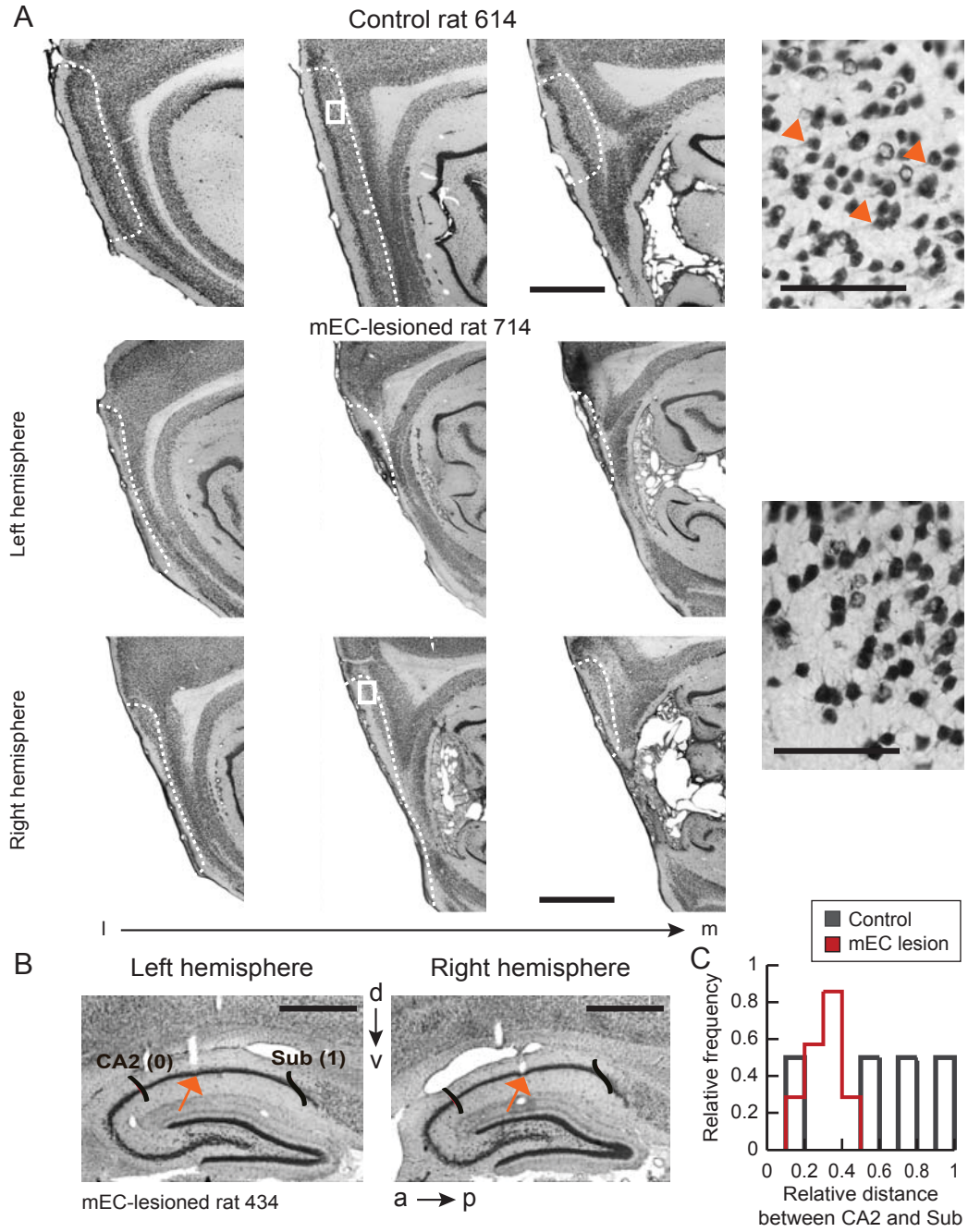

Figure S1. Example histological images of control and mEC-lesioned rats. Related to Figures 2–5. (**A**) Sagittal sections at three different lateral to medial levels are shown for one hemisphere in a control rat and for both hemispheres in mEC-lesioned rat 714. Superficial layers II and III are outlined by white stippled lines. The rightmost panel for each rat is a high-magnification image of layer III cells from the area indicated by a white box. Arrows in control image point to apical dendrites that are oriented towards the cortical surface. In the mEC-lesioned rat, cells in the superficial layers were either completely absent or, when small patches of cells were discernable, showed signs of disorganization and necrosis such as multipolar processes and fragmented nuclei. Scale bars are 1 mm and 125 µm. See Hales et al., 2014 and Schlesiger et al., 2015 for images from additional mEC-lesioned rats. (**B**) Tetrode tracks in the two hemispheres of mEC-lesioned rat 434 are shown in the sagittal plane. Arrows point to the end of tetrode tracks within the CA1 cell layer. (**C**) Distribution of relative tetrode locations along the proximal-to-distal axis. For each tetrode, the position between CA2 (0) and the subiculum (Sub, 1) was determined. In mEC-lesioned rats, all tetrodes were located in proximal to intermediate CA1.

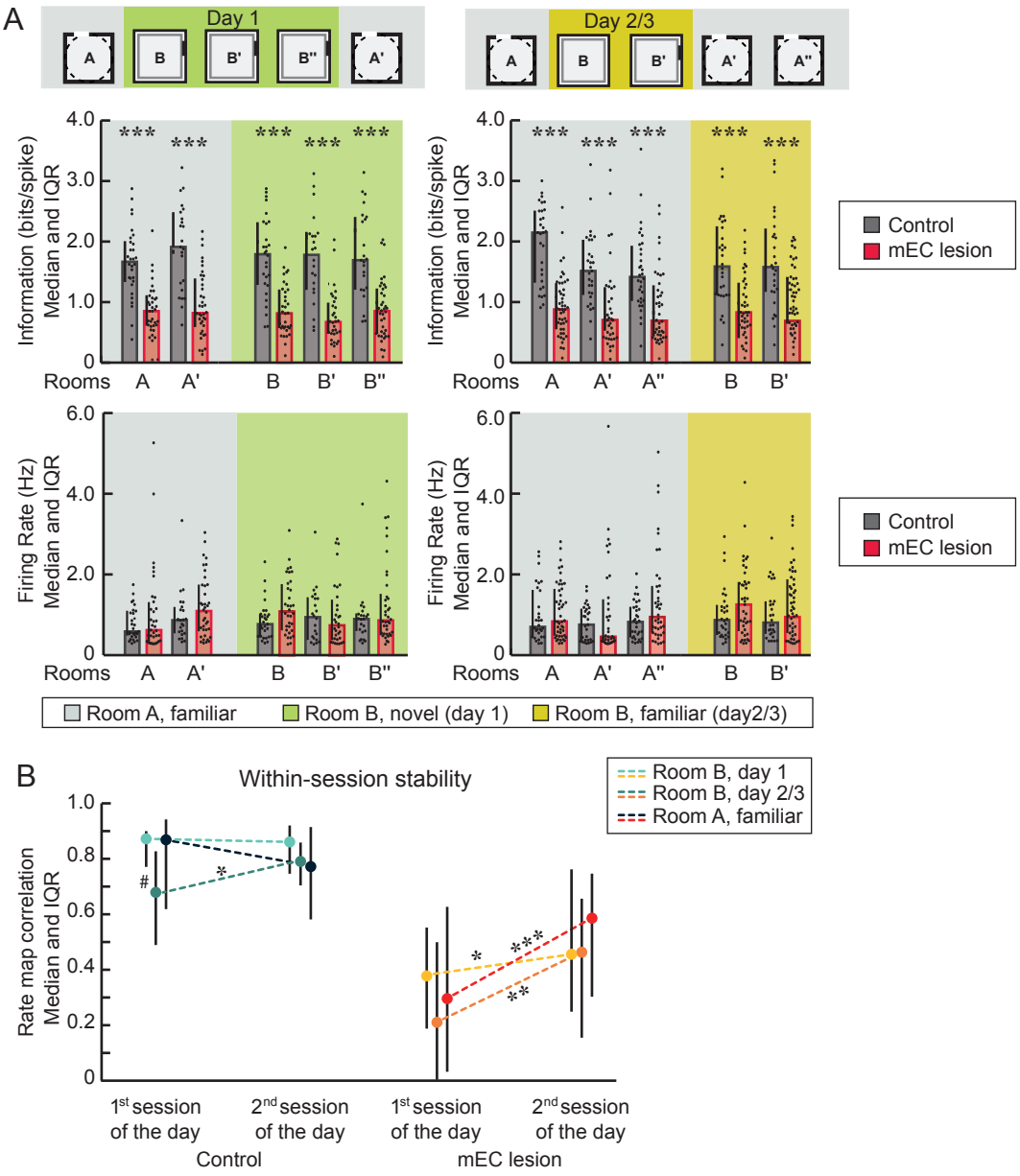

Figure S2. Information scores, mean firing rates and map stability in individual recording sessions. Related to Figure 2A. (**A**) Irrespective of the familiarity of the environment, information scores were reduced (all p values < 0.001, Mann-Whitney U tests), but firing rates were similar in mEC-lesioned compared to control rats (all p values ≥ 0.43, Mann-Whitney U tests). Black dots are values for individual cells, bars are medians, and error bars are IQR. *** $p \leq 0.001$, mEC lesioned vs control. (**B**) For three environments with different degrees of experience, the first and second 10-min session of the day was split into two 5-min intervals, and the within-session map stability was calculated. Of note, the within-session map stability in moderately and highly familiar environments in mEC-lesioned rats was as low as in entirely novel environments (p = 0.24, Kruskal-Wallis test). In controls, within-session map stability was lower in the first session of day 3 than in the other conditions (p = 0.00016, Kruskal-Wallis test). Within-session map stability increased from the first to the second session of the day in mEC-lesioned rats irrespective of the novelty of the environment (all p values ≤ 0.034, Wilcoxon signed-rank tests). Because stability was already high in the first session in control rats, there was no clear trend for a further increase (day 1 and highly familiar, both p values ≥ 0.099; day 3, p = 0.0099, Wilcoxon signed-rank tests). Symbols and error bars are the median and IQR. Holm-Bonferroni correction was applied for multiple comparisons. First vs. second session of the day, * $p \leq 0.05$, ** $p \leq 0.005$, *** $p \leq 0.001$; comparison between levels of familiarity, # $p \leq 0.001$.

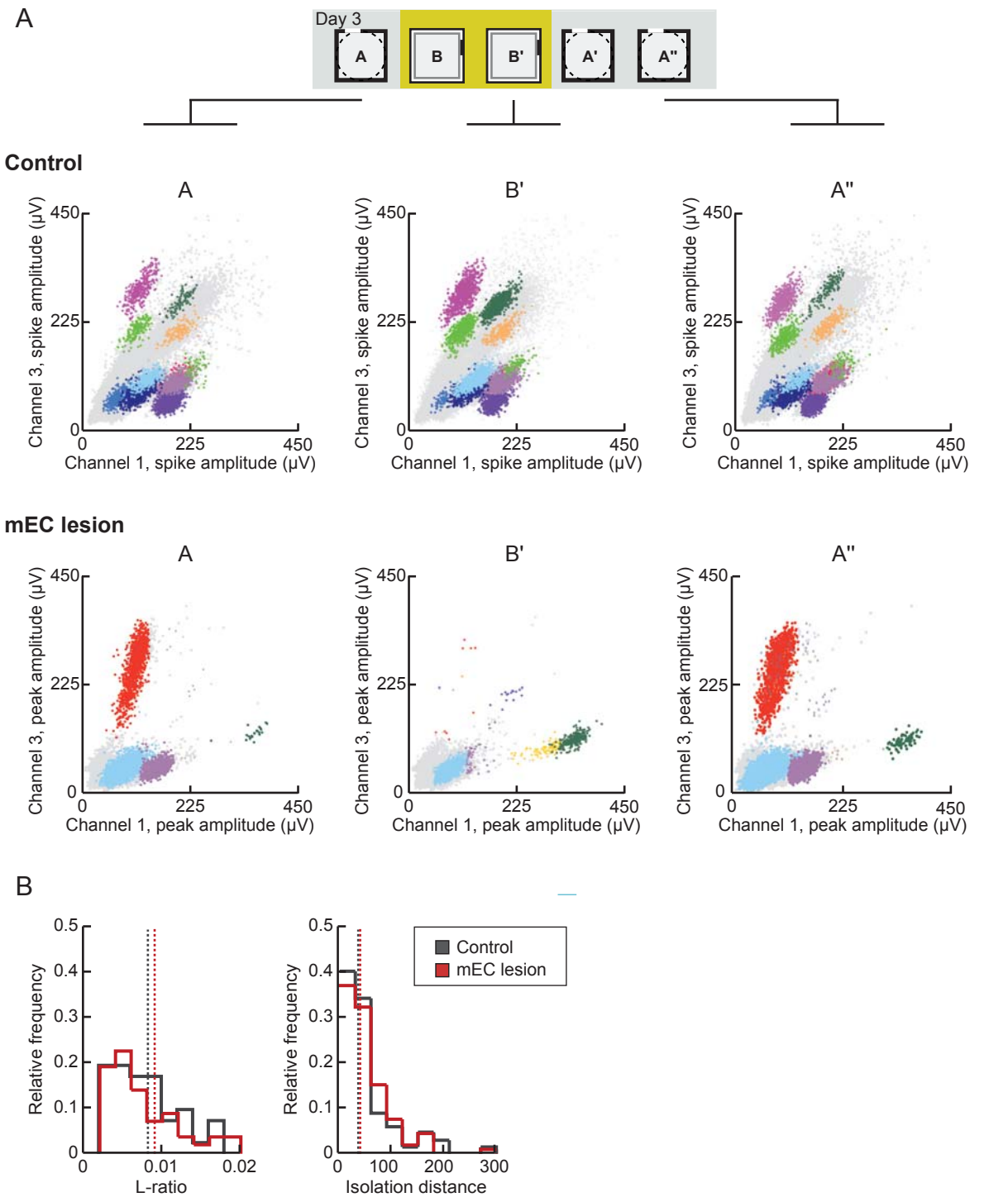

Figure S3. Cluster quality did not differ between control and mEC-lesioned rats. Related to Figure 2. (**A**) For each recording day, single-units were tracked across sessions. Scatter plots for spike amplitudes recorded on two of the four channels of a representative tetrode in a control (middle panel) and an mEC-lesioned rat (bottom panel) are shown for sessions A, B' and A'' of day three of the recording experiment. (**B**) Cluster quality measures did not differ between control and mEC-lesioned rats (L-ratio and Isolation distance, *p* values ≥ 0.43, Mann-Whitney U tests).

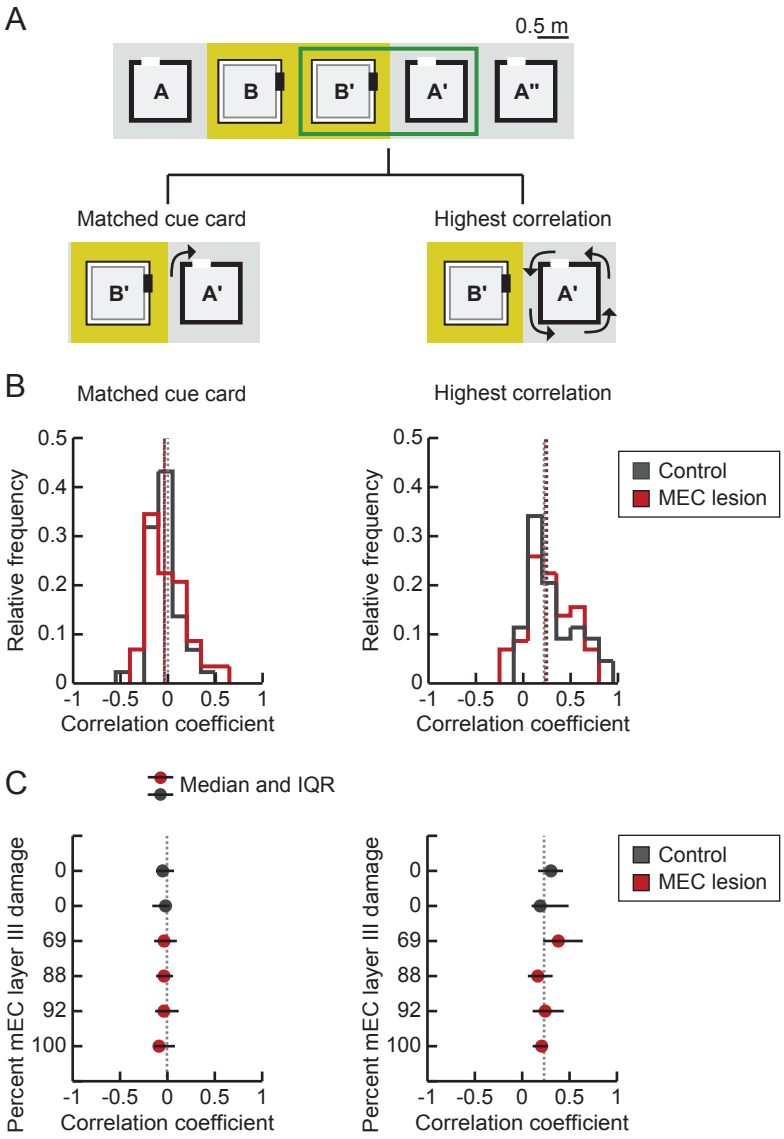

Figure S4. Low map similarity across rooms was not the result of the rotation of a stereotyped map. Related to Figure 4. (**A**) Schematic of the analysis performed to examine whether the low map similarity across rooms was the result of the coordinated shift of a constant map. For each cell, a pair of maps (top, green outline) was compared, after the map obtained in A' was rotated in one of two different ways. (1) It was rotated to match the orientation of the cue card across rooms (bottom left, 'Matched cue card'), or (2) it was rotated in steps of 90 degrees and the comparison with the highest correlation coefficient was selected for each cell (bottom right, 'Highest correlation'). To obtain the chance level, each analysis was repeated after shuffling of the cell identity. (**B**) In both the 'Matched cue card' and the 'Highest correlation' analysis, the median rate map correlation was similar between the control and mEC lesion groups (both *p*-values ≥ 0.65, Mann-Whitney U tests) and did not deviate from chance (stippled line) for either comparison (all *p*-values ≥ 0.37, Sign and Mann-Whitney U tests). None of the rats therefore demonstrated a coordinated shift of a constant map. (**C**) Circles represent the median rate map correlation coefficient per rat and are sorted by the extent of mEC III damage. In the 'Matched cue card' and the 'Highest correlation' analysis, the amount of remapping was similar when individual rats were compared to each other (all *p* values > 0.05, Kruskal-Wallis tests). In addition, map similarity was not different from chance in each individual control and mEC-lesioned rat (all *p* values > 0.05, Sign and Mann-Whitney U tests).

SUPPLEMENTAL EXPERIMENTAL PROCEDURES

Contact for Reagent and Resource Sharing

Further information and requests for resources may be directed to and will be fulfilled by the Lead Contact, Dr. Stefan Leutgeb (sleutgeb@ucsd.edu).

Experimental Model and Subject Details

Seven experimentally naïve, male, adult Long-Evans rats, obtained from Charles River Laboratories, were used for this experiment. Of these seven rats, five received mEC lesions and two received sham lesions. Previous publications included analysis from four of the five mEC-lesioned rats (Hales et al., 2014; Schlesiger et al., 2015), and information scores and firing rates during the first 10-min session on day 1 in the novel room were previously reported for these four rats (Hales et al., 2014). However, none of the remaining data from the recordings across rooms were included in previous publications. No animals were excluded for technical reasons. All experiments were performed in the dark phase of the cycle. During the experiment, rats were food restricted and maintained at ~90% of their free-feeding body weight. Water was available ad libitum. All experimental procedures were approved by the Institutional Animal Care and Use Committee at the University of California, San Diego.

Method Details

Surgical Procedures

Medial EC lesion surgeries and sham surgeries were performed as previously described (Hales et

al., 2014). In brief, to lesion the entire dorsoventral axis of the mEC, five rats received NMDA injections at eight different DV coordinates (-5.2, -4.7, -4.2, -3.7, -3.2, -2.7, -2.2, -1.7 mm) with an infusion rate of 0.1 µl/min (0.13 µl per site). The ML coordinate was ± 4.6 mm, and the needle was angled at 22° in the posterior to anterior direction, with the needle tip immediately anterior to the transverse sinus. In control rats, a craniotomy identical to the craniotomy in mEC-lesioned rats was performed, but dura was not punctured.

For hippocampal recordings, tetrodes were constructed by twisting four 17 µm polyimide-coated platinum-iridium (90%/10%) wires (California Fine Wire, California). The electrode tips were plated with platinum at 1 kHz to reduce the impedances to 200-300 kΩ. Fourteen tetrodes were arranged into two bundles, each containing six to eight independently movable tetrodes. After the mEC or sham lesion was made, the electrode assembly was secured to the skull using stainless steel screws and dental cement. The two tetrode bundles were targeted to the hippocampus of each hemisphere (AP: 4.0 mm, ML: ±2.45 mm, angled laterally towards CA1 recording sites at approximately ML ±3.0 mm). One electrode in each hemisphere remained in the cortex and was used as a reference for differential recordings.

Recording rooms, recording chambers and random foraging behavior

Three different rooms were introduced to each rat, except for rat 714 which was introduced to an additional room during a second series of recordings. In each room, the recording system and a light source were located in proximity to the entrance, and a recording chamber was placed on a table (54-66 cm height) that was located in the center of the room. Recording chambers were

either black or white squared boxes (1 m^2) or a black cylinder (diameter, 1 m) with 50 cm high walls. A polarizing cue card (20 x 50 cm) was placed in each recording chamber at a constant position. During foraging sessions, exploratory behavior was sustained by randomly scattering cereal crumbs over the surface area of the recording chamber at intervals of ~1 min. Before, in-between and after foraging sessions, the apparatus was cleaned with water while rats rested in a transparent holding box (30 cm x 30 cm x 56 cm) that was placed on a pedestal of 106 to 116 cm height. No curtains were used to allow the rat a free view of distal cues, such as posters on the wall and shelves.

Experimental design and recordings

Rats were pretrained for 5 days in two 10-min random foraging sessions per day. One control rat and four mEC-lesioned rats were also trained on a six-arm radial maze in the same room (as described in Schlesiger et al., 2013). Rats were subjected to either sham or mEC lesion surgery after pretraining was complete. After a recovery period of 7 days, training was continued in a second room for 7 to 12 days with two to six 10-min random foraging sessions per day. The rats trained on a six-arm maze before surgery were also trained on a six-arm maze after surgery. During the period of training, tetrodes were slowly advanced into the dorsal CA1 area of the hippocampus. After placing the majority of the tetrodes in the CA1 cell layer, hippocampal recordings were performed. During tetrode advancement and during recordings, the electrode assembly was connected to a multichannel, impedance matching, unity gain preamplifier headstage. The output was routed to a data acquisition system with 64 digitally programmable differential amplifiers (Neuralynx, Tucson, AZ, USA). Spike waveforms above a threshold of

40-45 µV were time-stamped and digitized at 32 kHz for 1 ms. The rat's position was tracked at 30 Hz by recording the position of light-emitting diodes that were placed above the head. Local field potentials were acquired by recording one channel of each tetrode with the filters set to the 1-450 Hz band.

Over 3 consecutive days, recording sessions included two different rooms on each day (Figure 1). Room A was familiar to the rats (room used for pretraining before surgery: control rats 505 and 614, mEC-lesioned rats 434 and 514; room used for training after surgery: mEC-lesioned rats 587 and 645). Room B was novel to the rats at the beginning of the recording sequence. Medial EC-lesioned rat 714 was tested in two sets of two-room experiments, in the room used for pretraining before surgery and a novel room as well as in the room used for training after surgery and a second novel room. Both novel rooms are referred to as room B for data analysis. Recordings from day 1 and day 3 were analyzed for all rats except when high quality recordings could not be obtained. Only data from day 1 were therefore included for rat 587, and recordings on day 2 instead of day 3 were analyzed for rat 434. On each recording day, a total of five recording sessions were performed across the two rooms (Figure 1). The foraging sessions were separated by inter-session intervals of 5 min, and the entire block of foraging sessions was preceded and followed by rest sessions of 10–20 min.

Histology

The brains were prepared for the identification of tetrode locations in cresyl violet-stained sections. For quantification of the mEC lesion extent, we also prepared NeuN-stained sections

(1:15000, Chemicon, CloneA60) and used the Cavalieri method as previously described (Hales et al., 2014) to measure the volume of the spared tissue in mEC layer II, mEC layer III, mEC deep layers, dorsal parasubiculum, ventral parasubiculum, and hippocampus. Patches of cells that showed clear signs of disorganization (e.g., multipolar processes in pyramidal layer III cells that have otherwise apical dendrites oriented toward the cortical cell surface) and necrosis (e.g., fragmented nuclei) were counted as damaged (see Figure S1).

Data analysis

All data analysis was performed by importing position and spike data into Matlab and by further processing the data with custom-written scripts and functions.

Spike sorting, cell tracking and cluster quality. Spike sorting was performed manually using the graphical cluster-cutting software (MClust, D. Redish), which we modified in order to reliably track clusters across sessions (Mankin et al., 2012). Recordings during rest periods throughout the day were used to confirm recording stability during the experiment and to identify hippocampal cells that were silent or fired at low rates during behavior. Clustering was performed manually in two-dimensional projections of a multidimensional parameter space (consisting of waveform amplitudes, waveform energies, and the peak-to-valley difference of each of the four tetrode channels). Autocorrelation and cross-correlation functions were used as additional separation tools. Putative principal cells were distinguished from putative interneurons by spike width and average firing rate, and only putative principal cells were included in the analysis. Cluster quality was assessed by calculating the L-ratio and the Mahalanobis (i.e., isolation) distance (Schmitzer-

Torbert et al., 2005) for each cluster of spikes recorded during the random foraging task.

Rate maps. The recording enclosure was divided into 5 cm x 5 cm location bins. Spatial firing rate distributions were constructed by summing the total number of spikes that occurred in each location bin, dividing the sum by the amount of time that the animal spent in that location, and then smoothing with a 5 by 5 bin Gaussian filter with a standard deviation of approximately 1 bin (Koenig et al. 2011).

Spatial correlation. The spatial similarity between rate maps across two rooms was calculated using Pearson's correlation. We first oriented trajectory maps obtained in each of the two rooms with respect to their allocentric orientation (i.e., the east wall of the recording chamber in room A was aligned with the east wall of the recording chamber in room B) and then centered the two maps with respect to each other. For each cell, the correlation coefficient was subsequently calculated by comparing the firing rates between all overlapping spatial bins. Similarly, rate maps between two sessions in the same room were compared by calculating the correlation coefficient between spatial bins at corresponding locations. For the within-session comparisons, the first and second 10-min session in each room (see Figure 1 for experimental design; novel room: B and B' on day 1 in room B; moderately familiar room: B and B' on day 3 in room B; highly familiar room: A' and A'' on day 3 of the recording sequence) was split into two 5-min intervals, and rate maps were generated for each of those intervals. The correlation coefficient was then calculated by comparing the first and second half of each session. For both the within and across-session comparison, cells that did not reach an average firing rate of ≥ 0.25 Hz in at least one of the two

compared sessions were excluded from analysis. The chance level was determined by shuffling the cell identity for each pair of sessions before calculating correlation coefficients. The shuffling procedure was repeated 100 times, and the median correlation coefficient was taken for each comparison (range of medians: -0.01 to 0.02).

The described approach was complemented with two additional methods. (1) The trajectory maps obtained in the two rooms were oriented with respect to the polarizing cue card (which was offset by either 90 or 270 degrees between the rooms) and the Pearson's correlation was subsequently calculated as described above. (2) For each cell, one of the maps was analytically rotated in steps of 90 degrees, the Pearson's correlation was calculated for each of the four possible comparisons, and the highest correlation coefficient from these comparisons was selected for further analysis.

Firing field boundaries. Place fields were defined by identifying areas of at least 8 adjacent pixels with a peak firing rate of at least 2 Hz. Starting from the peak, the field boundaries were found by building contours outwards until a threshold of 20% of the field's peak firing rate was reached. If any remaining peaks with a firing rate ≥ 2 Hz remained outside of an already defined field, the procedure was repeated. The field with the highest peak rate was retained as the cell's place field.

Distances between place fields. The distances between place field peaks were calculated for each pair of simultaneously recorded cells when each cell in the pair had at least one field over two consecutive recording sessions, either within the same room or across two different rooms

(within-room comparisons: day 3, A' and A''; across-room comparisons: day 3, A' and B'; see Figure 4A for schematic). Pearson's correlations were used to compare the place field distances between either two sessions in the same room (A' and A") or two sessions in different rooms (A' and B').

Spatial information. The information score was calculated for cells with average firing rates of ≥ 0.25 Hz. It describes the information density per spike and was calculated as described by Skaggs and colleagues (1993):

$$I = \sum_i p_i \frac{\lambda_i}{\lambda} \log_2 \frac{\lambda_i}{\lambda}$$

where I is the information density measured in bits per spike, i is the index of the pixels of the place field, P_i is the probability of the rat being at location i, λ_i is the average firing rate of the cell when the rat is at location i and λ is the total average firing rate.

Statistical analysis. All statistical tests were two-sided with $\alpha = 0.05$. To compare the proportion of active cells between groups, Chi-square tests were used. For all remaining statistical analysis, Kolmogorov-Smirnov tests were first performed to test for normality. Because all tested distributions were non-normal, equality of medians was tested with Mann-Whitney *U* tests and Kruskal-Wallis tests for between-group comparisons, and Wilcoxon signed-rank tests and Friedman tests for within-group comparisons. Sign tests were used to test the samples against chance. Multiple comparisons were corrected with the Holm-Bonferroni procedure, and Tukey-Kramer tests were used for post hoc analysis.

Resources Table

REAGENT or RESOURCE	SOURCE	IDENTIFIER
Antibodies		
Mouse monoclonal NeuN antibody	Chemicon	Clone A60
Biotinylated anti-mouse IgG	Vector BA-2000	
Biological Samples		
Chemicals, Peptides, and Recombinant Proteins		
Isoflurane	MWI	Cat #: NDC 13985-528-60
Buprenorphine	MWI	Cat #: 29308
Plantinic acid for platinum plating	Sigma-Aldrich	Cat #: 206083; CAS 18497-13-7
Sodium pentobarbital	MWI	Cat #: 15199
Formaldehyde	EMD	Cat #: FX-0415-4; CAS 50-00-0
Cresyl violet	EMD	Cat #: M-19012; CAS 10510-54-0
N-methyl-D-aspartate	Tocris	Cat #: 0114
Experimental Models: Organisms/Strains		
Long Evans rats	Charles River Labs	RRID: RGD_2308852
Software and Algorithms		
MClust	A.D. Redish	http://redishlab.neuroscience.umn.edu/MClust/MClust.html
Matlab v 2015b	Mathworks	RRID: SCR_001622
StereoInvestigator	MBF Bioscience	
Other		
Hyperdrive	Custom built; designed by B.L. McNaughton	US Patent: US5928143 A
Platinum-Iridium tetrode wire	California Fine Wire Company	Cat #: CFW0011873
Freezing microtome	Leica	Model: SM 2000R
Digital Neuralynx recording system	Neuralynx	Model: Digital Lynx SX

SUPPLEMENTAL REFERENCES

Koenig J., Linder A. N., Leutgeb J. K. & Leutgeb S. (2011). The spatial periodicity of grid cells is not sustained during reduced theta oscillations. *Science*, 332(6029):592-5.

Hales, J. B., Schlesiger, M. I., Leutgeb, J. K., Squire, L. R., Leutgeb, S. & Clark, R. E. (2014). Medial entorhinal cortex lesions only partially disrupt hippocampal place cells and hippocampus-dependent place memory. *Cell Rep,* 9**,** 893-901.

Mankin, E. A., Sparks, F. T., Slayyeh, B., Sutherland, R. J., Leutgeb, S. & Leutgeb, J. K. (2012). Neuronal code for extended time in the hippocampus. *Proc Natl Acad Sci U S A,* 109**,** 19462-7.

Skaggs, W. E., McNaughton, B. L., Gothard, K. M. & Markus, E. J. (1993). An information-theoretic approach to deciphering the hippocampal code. *Advances in Neural Information Processing Systems 5* (eds. Hanson, S. J., Giles, C. L. & Cowan, J. D.) 1030-1037 (Morgan Kaufmann, San Mateo).

Schlesiger, M. I., Cannova, C. C., Boublil, B. L., Hales, J. B., Mankin, E. A., Brandon, M. P., Leutgeb, J. K., Leibold, C. & Leutgeb, S. (2015). The medial entorhinal cortex is necessary for temporal organization of hippocampal neuronal activity. *Nat Neurosci*, 18, 1123-32.

Schlesiger, M. I., Cressey, J. C., Boublil, B., Koenig, J., Melvin, N. R., Leutgeb, J. K. & Leutgeb, S. (2013). Hippocampal activation during the recall of remote spatial memories in radial maze tasks. *Neurobiol Learn Mem,* 106**,** 324-33.

Schmitzer-Torbert N., Jackson J., Henze D., Harris K. & Redish A. D. (2005). Quantitative measures of cluster quality for use in extracellular recordings. *Neuroscience*, 131(1): 1-11.